

# MOLPIPx: an end-to-end differentiable package for permutationally invariant polynomials in Python and Rust

Manuel S. Drehwald,<sup>1,2, a)</sup> Asma Jamali,<sup>3,2, a)</sup> and Rodrigo A. Vargas-Hernández<sup>2,3,4</sup>

<sup>1)</sup>*Department of Computer Science, University of Toronto, Toronto, ON, Canada*

<sup>2)</sup>*Department of Chemistry and Chemical Biology, McMaster University, Hamilton, ON, Canada*

<sup>3)</sup>*School of Computational Science and Engineering, McMaster University, Hamilton, ON, Canada*

<sup>4)</sup>*Brockhouse Institute for Materials Research, McMaster University, Hamilton, ON, Canada*

(\*Electronic mail: [vargashr@mcmaster.ca](mailto:vargashr@mcmaster.ca))

In this work, we present MOLPIPx, a versatile library designed to seamlessly integrate Permutationally Invariant Polynomials (PIPs) with modern machine learning frameworks, enabling the efficient development of linear models, neural networks, and Gaussian process models. These methodologies are widely employed for parameterizing potential energy surfaces across diverse molecular systems. MOLPIPx leverages two powerful automatic differentiation engines—JAX and EnzymeAD-Rust—to facilitate the efficient computation of energy gradients and higher-order derivatives, which are essential for tasks such as force field development and dynamic simulations. MOLPIPx is available at <https://github.com/ChemAI-Lab/molpipx>.

## I. INTRODUCTION

The construction of potential energy surfaces (PESs) has been a long challenge in the computational chemistry community<sup>1–14</sup>. One of the most successful methodologies, permutationally invariant polynomials (PIPs), has a history of over 20 years and has inspired numerous reviews due to its success<sup>15–23</sup>. PIPs offer a unique approach to representing the structural information of molecules by ensuring invariance between permutations of like atoms within a molecule<sup>24,25</sup>. This property is pivotal, as it allows models to effectively discern molecular features regardless of atom ordering, creating robust and efficient regression models<sup>25,26</sup>. Given the flexibility of PIP models, they have also been adapted for the computation of the forces<sup>26–30</sup> which has allowed their use in molecular dynamic simulations<sup>28,31–36</sup>.

To date, more than 100 PIP-based PESs have been developed<sup>25</sup>. Early examples of PIPs<sup>37</sup> for PESs are  $\text{CH}_5$ <sup>38</sup>,  $\text{H}_5$ <sup>39</sup>, and the chemical reaction  $\text{H} + \text{CH}_4$ <sup>40</sup>. Subsequently, PIP models were developed for molecules with 7 or more atoms, including ethanol<sup>41</sup>, nitromethane<sup>42</sup>, formic acid dimer<sup>43</sup>, glycine<sup>44</sup>, N-methyl acetamide<sup>29,45,46</sup>, acetylacetone<sup>47</sup>, and tropolone<sup>48</sup>, as well as for the 4 water molecules<sup>49</sup>. In addition, PIPs have been used in the MB-pol-like potentials<sup>50–55</sup>, and other many-body type potentials for solvated molecules like  $\text{CO}_2/\text{H}_2\text{O}$ <sup>56</sup>. Recently, Bowman et al.<sup>57</sup> published the first in a series of papers focused on alkanes of the form  $\text{C}_n\text{H}_{2n+2}$ , with a particular emphasis on  $\text{C}_{14}\text{H}_{30}$ . A ROBOSURFER program has been used to study reactions like  $\text{CH}_3\text{Br} + \text{F}^-$  using PIPs via automating the selection of new geometries, performing *ab initio* computations, and iteratively refining the PES<sup>58</sup>. A method involving dictionary learning with "greedy" selection reduces the basis size with minimal accuracy loss and can automatically

generate PIPs for complex systems using parallelization<sup>59,60</sup>. Additionally, a permutationally invariant method using an "n-body" representation has been introduced for polyatomic molecules<sup>61</sup>. Several PESs, including  $\text{N} + \text{N}_2$ <sup>62</sup>,  $\text{N} + \text{O}_2$ <sup>63</sup> and  $\text{N}_2 + \text{N}_2$ <sup>64</sup>, have been studied using PIPs, with frameworks that remove "disconnected" terms, achieving purification and compaction<sup>59,60,65</sup>. With the growth of computational power, PIPs have been recently adapted to study materials that rely on high-dimensional PESs<sup>66–68</sup>.

Researchers have also explored different methodologies to effectively incorporate PIPs with modern machine learning (ML) models<sup>69,70</sup> like neural networks (NNs) and Gaussian Processes (GPs), for example, the PES-Learn software<sup>71</sup>. With fairly successful results, researchers have shifted towards assessing the performance of these various models using specific molecules such as  $\text{H}_3\text{O}_2$ <sup>26</sup>,  $\text{CH}_4$ <sup>28</sup>,  $\text{H}_3\text{O}^+$ <sup>37,72</sup> and  $\text{C}_2\text{H}_6\text{O}^73$ , to mention a few<sup>45,46</sup>.

PIPs were first integrated with neural networks to construct PESs for gas-phase molecules<sup>74</sup> starting with triatomic<sup>75,76</sup> ( $\text{H} + \text{H}_2$  and  $\text{Cl} + \text{H}_2$ ) and tetratomic<sup>77–79</sup> ( $\text{X} + \text{H}_2\text{O} \rightarrow \text{HX} + \text{H}_2\text{O}$  ( $\text{X} = \text{H}, \text{F}, \text{O}$ )) systems and later extended to several polyatomic systems<sup>76,80–84</sup>. This framework has also been applied to molecular systems, like Criegee intermediates ( $\text{CH}_2\text{OO}$ <sup>85,86</sup> and dioxirane<sup>87</sup>), acetylene-vinylidene<sup>88</sup>, and the  $\text{H}_2\text{CC}^-$  anion<sup>89</sup>. Furthermore, this approach was further extended to molecular surfaces like  $\text{H}_2 + \text{Cu(III)}$  and  $\text{H}_2 + \text{Ag(III)}$ <sup>90</sup>. For more details regarding the integration of PIPs in NN, we refer the reader to the review by S. Manzhos, Sergei et al.<sup>91</sup>. Given the flexibility of NN, this combined framework has been extended to diabatic potential energy matrices<sup>92,93</sup>. In addition, the combination of PIP, neural network, and  $\Delta$ -machine learning shows a robust and efficient approach for constructing highly accurate PESs across various molecular systems, from simple diatomic dissociations to complex multi-atom reactions<sup>94</sup>.

The other successful integration of ML models with PIPs is when combined with Gaussian processes. This framework has been applied to various molecular systems, including  $\text{H}_3\text{O}^+$ ,

<sup>a)</sup>These authors contributed equally.

OCHCO<sup>+</sup>, (HCOOH)<sub>2</sub>, and H<sub>2</sub>CO/HCOH, demonstrating its efficacy in terms of fitting accuracy, computational efficiency, and the ability to capture PES features such as stationary points and harmonic frequencies<sup>95</sup>.

Given the extensive use of PIPs in materials science and computational chemistry, we present MOLPIPx, a flexible library that can seamlessly integrate PIPs with advancements in machine learning modelling, enhancing the simulation of a wide range of chemical systems. MOLPIPx takes advantage of two main automatic differentiation engines, JAX for the Python version and Enzyme-AD<sup>96–98</sup> for the Rust version.

## II. MODELS

This section describes the three main regression models in the MOLPIPx library. First, Sections II B and II C introduce PIPs under the framework of function composition and its extension to linear models for PESs. This is followed by discussing PIPs’ integration with ML algorithms, specifically neural networks and Gaussian Processes, Sections II D and II E. For more details regarding the PIP framework, we encourage the reader to consult Refs.<sup>24,25,45,46,99</sup>. The general structure of MOLPIPx and its components is depicted in Fig. 1.

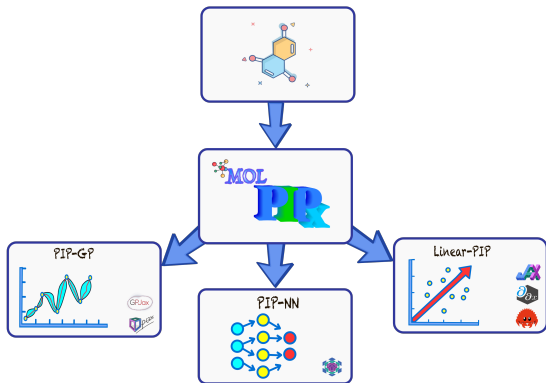


FIG. 1. Overview of the MOLPIPx package. For any model developed under MOLPIPx, the monomial and polynomial functions are constructed using the MSA algorithm and then translated into JAX or Rust, depending on the selected back-end. We provide some monomial and polynomial functions, see Table I. The input for all models is the Cartesian coordinates of a molecule, which are used to construct the PIP vector (Eq. 1). These vectors can then be integrated into other modern machine learning models to build PESs.

### A. Permutationally Invariant Polynomial Representation

The PIP representation for PES models can be conceptually described as a complex composition of multiple functions that transform the Cartesian coordinates of a molecule ( $\mathbf{x}$ ) into a structured vector ( $\Phi_{\text{PIP}}$ ), which is invariant to permutations of similar nuclei. The primary motivation for articulating  $\Phi_{\text{PIP}}$  as a sequence of function compositions is to facilitate its integration with modern automatic differentiation frameworks

(AD)<sup>100</sup>. AD has been fundamental in the numerical ecosystem of deep learning libraries and, more recently, in computational chemistry simulations.<sup>100–114</sup> By structuring the PIP vector, each component function can be seamlessly differentiated and combined with other machine learning algorithms; Sections II D and II E.

The construction of  $\Phi_{\text{PIP}}$  in MOLPIPx begins with calculating the inter-nuclei distances ( $\mathbf{r}$ ), which are then transformed into Morse variables ( $\bar{\gamma}$ )<sup>24</sup>. The subsequent steps involve computing the symmetrized monomials ( $\mathbf{z}_{\text{mono}}$ ) and polynomials ( $\mathbf{z}_{\text{poly}}$ ) using the  $f_{\text{mono}}$  and  $f_{\text{poly}}$  functions. These groups of transformations ensure that the resulting representation is invariant under the permutation of identical nuclei, thus capturing the correct molecular symmetries. Mathematically, the  $\Phi_{\text{PIP}}$  vector can be defined as follows,

$$\Phi_{\text{PIP}}(\mathbf{x}) = (f_{\text{poly}} \circ f_{\text{mono}} \circ \gamma \circ d)(\mathbf{x}), \quad (1)$$

where each component in this composition of functions represents a non-linear transformation defined as,

$$\mathbf{r} = d(\mathbf{x}), \quad (\text{inter-nuclei distances}) \quad (2)$$

$$\bar{\gamma} = \gamma(\mathbf{r}) = e^{-\lambda \mathbf{r}}, \quad (\text{Morse variables}) \quad (3)$$

$$\mathbf{z}_{\text{mono}} = f_{\text{mono}}(\bar{\gamma}), \quad (\text{symmetrized monomials}) \quad (4)$$

$$\mathbf{z}_{\text{poly}} = f_{\text{poly}}(\mathbf{z}_{\text{mono}}) \quad (\text{symmetrized polynomials}). \quad (5)$$

In Eq. 3,  $\lambda$  is a length-scale hyper-parameter, and the  $f_{\text{mono}}$  and  $f_{\text{poly}}$  functions are constructed using the monomial symmetrization algorithm (MSA)<sup>99</sup>.

### B. Linear Permutationally Invariant Polynomial Models

Linear regression frameworks are the most commonly used strategies for building PIP models for PESs, and are defined as,

$$y(\mathbf{x}) = \mathbf{w}^\top \Phi_{\text{PIP}}(\mathbf{x}) = \sum_{i=1}^{n_p} w_i \phi_i(\mathbf{x}), \quad (6)$$

where  $y$  represents the potential energy,  $\mathbf{w}$  denotes the linear weights, and  $n_p$  is the number of elements in  $\Phi_{\text{PIP}}$  given a polynomial degree  $p$ . The optimization of  $\mathbf{w}$  is typically achieved using least-squares methods, and as detailed in Ref.<sup>28</sup>, it can be adapted to include the forces by incorporating the Jacobian of  $\Phi_{\text{PIP}}$  for each geometry ( $\nabla_{\mathbf{x}_i} \Phi_{\text{PIP}}$ ) in the least-squares equation,

$$\begin{bmatrix} \phi_0(\mathbf{x}_1) & \phi_1(\mathbf{x}_1) & \cdots & \phi_{n_p}(\mathbf{x}_1) \\ \vdots & \vdots & & \vdots \\ \phi_0(\mathbf{x}_N) & \phi_1(\mathbf{x}_N) & \cdots & \phi_{n_p}(\mathbf{x}_N) \\ \frac{\partial \phi_0(\mathbf{x}_1)}{\partial x_1} & \frac{\partial \phi_1(\mathbf{x}_1)}{\partial x_1} & \cdots & \frac{\partial \phi_{n_p}(\mathbf{x}_1)}{\partial x_1} \\ \vdots & \vdots & & \vdots \\ \frac{\partial \phi_0(\mathbf{x}_1)}{\partial x_{3n_a}} & \frac{\partial \phi_1(\mathbf{x}_1)}{\partial x_{3n_a}} & \cdots & \frac{\partial \phi_{n_p}(\mathbf{x}_1)}{\partial x_{3n_a}} \\ \vdots & \vdots & & \vdots \\ \frac{\partial \phi_0(\mathbf{x}_N)}{\partial x_1} & \frac{\partial \phi_1(\mathbf{x}_N)}{\partial x_1} & \cdots & \frac{\partial \phi_{n_p}(\mathbf{x}_1)}{\partial x_1} \\ \vdots & \vdots & & \vdots \\ \frac{\partial \phi_0(\mathbf{x}_N)}{\partial x_{3n_a}} & \frac{\partial \phi_1(\mathbf{x}_N)}{\partial x_{3n_a}} & \cdots & \frac{\partial \phi_{n_p}(\mathbf{x}_N)}{\partial x_{3n_a}} \end{bmatrix} \begin{bmatrix} w_0 \\ w_1 \\ w_2 \\ \vdots \\ w_\ell \\ \vdots \\ w_{n_p-1} \\ w_{n_p} \end{bmatrix} = \begin{bmatrix} y(\mathbf{x}_1) \\ \vdots \\ y(\mathbf{x}_N) \\ \frac{\partial y(\mathbf{x}_1)}{\partial x_1} \\ \vdots \\ \frac{\partial y(\mathbf{x}_1)}{\partial x_{3n_a}} \\ \vdots \\ \frac{\partial y(\mathbf{x}_N)}{\partial x_1} \\ \vdots \\ \frac{\partial y(\mathbf{x}_N)}{\partial x_{3n_a}} \end{bmatrix}, \quad (7)$$

where  $n_a$  is the total number of atoms in the molecule.

From Eq. 7, it becomes evident that there is a need for an efficient and robust framework to compute  $\nabla_{\mathbf{x}} \Phi_{\text{PIP}}$  and forces ( $\nabla_{\mathbf{x}} \mathbf{w}^\top \Phi_{\text{PIP}}$ ). Because of this and the wide use of PIP for PESs, there have been previous attempts to make PIP models fully differentiable using both, forward<sup>28</sup> and reverse<sup>30</sup> mode differentiation. For  $\nabla_{\mathbf{x}} \Phi_{\text{PIP}}$ , a forward mode approach may be memory more efficient, particularly when  $n_p$  is large. However, reverse mode differentiation enables the computation of both the energy and force at the same cost as evaluating the energy<sup>100</sup>. These AD-like frameworks are custom-developed solely for linear PIP models, thus limiting their integration with other regression models and tasks that require higher-order derivatives.

### C. Anisotropic Morse Variables

One of the foundational components of  $\Phi_{\text{PIP}}$  is the Morse variables,  $\tilde{\gamma}$ , which are modulated by the length-scale hyperparameter  $\lambda$ . Typically, a uniform  $\lambda$  is applied across all inter-nuclei distances. Inspired by automatic relevance determination methods in kernel machines<sup>115</sup>, we introduce an anisotropic formulation of the Morse variables, where unique length-scale parameters are assigned to each type of atom-atom distance. For example, in ammonia ( $\text{NH}_3$ ), which contains two different types of distances, H–H and N–H, the distinct length-scale parameters are  $\lambda_{\text{HH}}$  and  $\lambda_{\text{NH}}$ . This approach ensures that each  $\lambda_\ell$  parameter exclusively affects its corresponding distance type, maintaining permutational invariance. Following Eq. 1 notation, we define  $\Phi_{\text{PIP}}^{\text{aniso}}$  as a PIP model with anisotropic Morse variables as,

$$\Phi_{\text{PIP}}^{\text{aniso}}(\mathbf{x}) = (f_{\text{poly}} \circ f_{\text{mono}} \circ \gamma_{\text{aniso}} \circ d)(\mathbf{x}), \quad (8)$$

where the anisotropic Morse variables are defined by,

$$\tilde{\gamma}_{\text{aniso}} = \gamma_{\text{aniso}}(\lambda, \omega, \mathbf{r}) = \exp\left(-\sum_{\ell} \lambda_{\ell} \omega_{\ell} \odot \mathbf{r}\right), \quad (9)$$

here,  $\odot$  denotes the Hadamard product between the distance vector  $\mathbf{r}$  and the mask vector<sup>116</sup>  $\omega_{\ell}$ , and the sum  $\sum_{\ell}$  is over the unique types of inter-nuclei distances. The mask vector elements ( $\omega_{\ell,j}$ ) are defined as,

$$\omega_{\ell,j} = \begin{cases} 1 & \text{if } r_j \text{ is the same type as } \lambda_{\ell}, \\ 0 & \text{otherwise.} \end{cases} \quad (10)$$

In isotropic  $\Phi_{\text{PIP}}$  models, the value of  $\lambda$  can be optimized with grid search methods or Bayesian optimization<sup>117–119</sup>. Instead of relying on these sampling optimization algorithms and following Ref.<sup>101</sup>, we leverage a fully differentiable pipeline and utilize a gradient-based optimization algorithm for the joint optimization of a two-loss function setup,

$$\begin{aligned} \lambda^* &= \arg \min_{\lambda \in \mathbb{R}} \mathcal{L}_{\text{outer}}(\tilde{\mathbf{w}}(\lambda)) \\ \text{subject to } & \tilde{\mathbf{w}}(\lambda) = \arg \min_{\mathbf{w} \in \mathbb{R}} \mathcal{L}_{\text{inner}}(\mathbf{w}, \lambda), \end{aligned} \quad (11)$$

where  $\mathcal{L}_{\text{outer}}$  is the validation loss function, and  $\mathcal{L}_{\text{inner}}$  is the training loss function that jointly depends on  $\lambda$  and  $\mathbf{w}$ . Here,  $\tilde{\mathbf{w}}(\lambda)$  denotes the optimal solution of  $\mathcal{L}_{\text{inner}}$ , typically solved using least-squares methods, Eq. 7. To efficiently solve for  $\lambda^*$ , and because of the chain rule, it is essential to determine the gradient  $\frac{\partial \tilde{\mathbf{w}}}{\partial \lambda}$ . This gradient can be effectively calculated using implicit differentiation techniques<sup>101,113</sup>, enabling a systematic and efficient approach to optimizing the anisotropic model parameters for molecular systems with a higher number of unique types of inter-nuclei distances.

### D. Permutationally Invariant Polynomial Neural Networks

Feed-forward neural networks (NNs) known also as multi-layer perceptrons, have been used for PESs<sup>91,120</sup>. However, when modeling PESs, neural networks encounter limitations as they do not inherently accommodate the permutation of identical nuclei. Addressing this gap, the integration of PIPs within NNs, coined as PIP-NN ( $f_{\text{PIP-NN}}$ ), was pioneered by B. Jiang et al. in Ref.<sup>75</sup>. This innovative approach significantly enhances neural networks by embedding the necessary symmetry considerations using  $\Phi_{\text{PIP}}$  as a symmetrized input to the overall model<sup>121,122</sup>. Following the same framework of function composition, PIP-NNs can be defined as,

$$f_{\text{PIP-NN}}(\mathbf{x}) = (f_{\text{NN}} \circ \Phi_{\text{PIP}})(\mathbf{x}), \quad (12)$$

where  $f_{\text{NN}}$  can be any NN architecture, commonly feed-forward NNs are the most used NN architecture,

$$f_{\text{NN}}(\mathbf{x}) = (g_L \circ \dots \circ g_1 \circ \Phi_{\text{PIP}})(\mathbf{x}), \quad (13)$$

where  $L$  represents the number of layers, and each layer  $g_\ell$  is parametrized by,

$$g_\ell(\mathbf{z}) = \sigma(\mathbf{w}_\ell \mathbf{z} + b_\ell), \quad (14)$$

where  $\sigma$  is the activation function, and  $\{\mathbf{w}_\ell, b_\ell\}_{\ell=1}^L$  represent the set of parameters for the PIP-NN model.

For PESs, it is a standard practice to train PIP-NNs using both forces and energies jointly,

$$\begin{aligned} \mathcal{L}(\Theta, \lambda_0) &= \frac{1}{N} \sum_i \|\nabla f_{\text{PIP-NN}}(\mathbf{x}_i) - \nabla V(\mathbf{x}_i)\|_2 \\ &+ \lambda_0 (f_{\text{PIP-NN}}(\mathbf{x}_i) - V(\mathbf{x}_i))^2, \end{aligned} \quad (15)$$

where the  $\lambda_0$  hyper-parameter determines the relative weighting between the energy ( $f_{\text{PIP-NN}}(\mathbf{x})$ ) and force ( $\nabla f_{\text{PIP-NN}}(\mathbf{x})$ ) terms, helping to account for differences in their magnitudes. PIP-NNs, like other neural network-based PES models, function as force-field models that train efficiently using stochastic gradient descent methods, with the gradient  $\nabla f_{\text{PIP-NN}}(\mathbf{x})$  computed through automatic differentiation (AD).

### E. Permutationally Invariant Polynomial Gaussian Process

Gaussian Process (GP) models<sup>115,123–125</sup> have become one of the most prominent regression models for PESs, and have

recently been adapted for larger molecular systems<sup>126–137</sup>. A GP, denoted as  $V(\mathbf{x}) \sim \mathcal{GP}(\boldsymbol{\mu}, \boldsymbol{\Sigma})$ , is characterized by its mean ( $\boldsymbol{\mu}$ ) and covariance function ( $\boldsymbol{\Sigma}$ ), which is parameterized by the kernel function  $k(\mathbf{x}_i, \mathbf{x}_j)$ . The kernel function is a critical component as it describes the similarity between the data points.

A significant advantage of GPs over other probabilistic regression models is their ability to provide a closed-form solution for the posterior distribution with mean and standard deviation functions given by,

$$\boldsymbol{\mu}(\mathbf{x}) = k(\mathbf{x}, \mathbf{X})^\top [K(\mathbf{X}, \mathbf{X}) + \sigma_n \mathbb{I}]^{-1} \mathbf{y}, \quad (16)$$

$$\boldsymbol{\sigma}(\mathbf{x}) = -k(\mathbf{x}, \mathbf{X})^\top [K(\mathbf{X}, \mathbf{X}) + \sigma_n \mathbb{I}]^{-1} k(\mathbf{x}, \mathbf{X}) + k(\mathbf{x}, \mathbf{x}), \quad (17)$$

where for PESs  $\mathbf{X}$  and  $\mathbf{y}$  represent the geometric configurations and the corresponding energies. In GPs, the kernel function depends on training parameters ( $\boldsymbol{\theta}$ ) that are optimized by maximizing the logarithm of the marginal likelihood (LML),

$$\log p(\mathbf{y}|\mathbf{X}, \boldsymbol{\theta}) = -\frac{1}{2} \mathbf{y}^\top [K(\mathbf{X}, \mathbf{X}) + \sigma_n \mathbb{I}]^{-1} \mathbf{y} - \frac{1}{2} \log |K(\mathbf{X}, \mathbf{X}) + \sigma_n \mathbb{I}| - \frac{N}{2} \log 2\pi. \quad (18)$$

For further details regarding GPs, we refer the reader to Refs.<sup>115,117</sup>.

As discussed in Refs.<sup>115,122</sup>, to construct a GP that accurately represents an invariant function, the kernel must also be invariant. Following the approach of C. Qu *et al.* in Ref.<sup>95</sup>, we define PIP-GPs, as models where  $\Phi_{\text{PIP}}$  is used in the kernel function,

$$k(\mathbf{x}_i, \mathbf{x}_j) = k(\Phi_{\text{PIP}}(\mathbf{x}_i), \Phi_{\text{PIP}}(\mathbf{x}_j)), \quad (19)$$

where  $k$  can be any standard kernel such as Radial basis function (RBF) or Matérn, ensuring the covariance matrix  $K$  is symmetric and positive semi-definite. Eq. 19 formulation is kin with the 'Deep Kernel Learning' framework,<sup>138</sup> commonly used in contemporary GPs, where NNs parameterize the latent representation of the inputs, followed by the RBF or similar kernel functions. The training of these GP models can proceed similarly to standard GPs, using gradient-based methods to maximize the LML (Eq. 18). The gradient of the LML with respect to the parameters of  $k$  can be computed via automatic differentiation, a common feature in modern GP libraries like GPyTorch<sup>139</sup>, GPJax<sup>140</sup>, and GAUCHE<sup>141</sup>. Additionally, using automatic differentiation, one can compute the derivative of  $\boldsymbol{\mu}(\mathbf{x})$  with respect to  $\mathbf{x}$  to determine the forces for PESs<sup>142,143</sup>.

### III. SOFTWARE ARCHITECTURE

At its core, the library consists of an implementation of the  $f_{\text{mono}}$  and  $f_{\text{poly}}$  functions compatible with two automatic differentiation back-ends, e.g., JAX<sup>144</sup> and EnzymeAD-Rust, and is openly available at <https://github.com/ChemAI-Lab/molpipx>. MOLPIPx relies on the MSA package

developed by Bowman and co-workers, accessible at <https://github.com/szquchen/MSA-2.0>, to generate the monomial and polynomial files, which are then translated into a format compatible with the selected back-end using the `msa_file_generator` function. This workflow is illustrated in Fig. 2 and Listing 1 for the water molecule ( $A_2B$  symmetry). Listings 2 and 3 provide examples of the monomial and polynomial functions for the  $A_2B$  molecule in JAX, translated from the MSA using MOLPIPx. For user convenience, the MOLPIPx library includes pre-configured  $f_{\text{mono}}$  and  $f_{\text{poly}}$  functions for the molecules listed in Table I. The molecules listed in Table I adhere to a general symmetry notation. For instance,  $A_3$  represents the  $\text{H} + \text{H}_2 \longrightarrow \text{H}_2 + \text{H}$  reaction, while water and methane correspond to  $A_2B$  and  $A_4B$ , respectively. These monomial and polynomial functions are also compatible with models based on the many-body expansion.

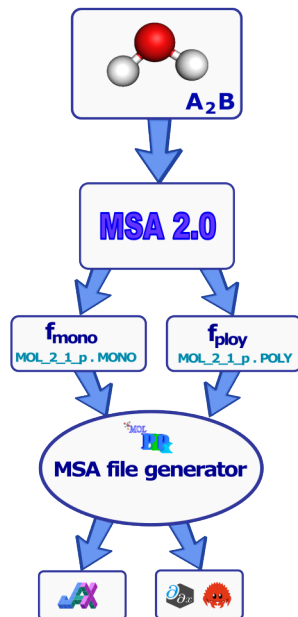


FIG. 2. Overview of the workflow to construct the  $f_{\text{mono}}$  and  $f_{\text{poly}}$  functions for the selected back-end. The MOLPIPx library translates the `MOL_symm_p.MONO` and `MOL_symm_p.POLY` files generated using the MSA package.

```
1 from molpipx.pip_generator import msa_file_generator
2 path = './'
3 files_msa = 'MOL_2_1_3' # name of the msa files
4 label = 'A2B_p_3' # name of the output files
5 # generate mono and poly files in jax
6 msa_file_generator(files_msa, path, label)
```

Listing 1. Monomial and polynomial files generator for an  $A_2B$  molecule.

```
1 import jax.numpy as jnp
2 from jax import jit
3 @jit
4 def f_mononials(r):
5     mono_0 = 1.
6     mono_1 = jnp.take(r, 2)
7     mono_2 = jnp.take(r, 1)
8     mono_3 = jnp.take(r, 0)
```

TABLE I. List of molecules available in the MOLPIPx Library. For each molecule listed, MOLPIPx has polynomial degrees ranging from 3 to 7.

Molecule	
A <sub>3</sub>	A <sub>5</sub>
A <sub>2</sub> B	A <sub>4</sub> B
ABC	A <sub>3</sub> B <sub>2</sub>
A <sub>4</sub>	A <sub>3</sub> BC
A <sub>3</sub> B	A <sub>2</sub> B <sub>2</sub> C
A <sub>2</sub> B <sub>2</sub>	A <sub>2</sub> BCD
A <sub>2</sub> BC	ABCDE
ABCD	

```

9 mono_4 = mono_1 * mono_2
10 return jnp.stack([mono_0, mono_1, mono_2,
11                  mono_3, mono_4])

```

Listing 2. Monomial function for A<sub>2</sub>B molecule.

```

1 import jax.numpy as jnp
2 from jax import jit
3 from monomial_file import f_monomials as f_mono
4 @jit
5 def f_polynomials(r):
6     mono = f_monos(r.ravel())
7     poly_0 = jnp.take(mono, 0)
8     poly_1 = jnp.take(mono, 1) + jnp.take(mono, 2)
9     poly_2 = jnp.take(mono, 3)
10    poly_3 = jnp.take(mono, 4)
11    poly_4 = poly_2 * poly_1
12    poly_5 = poly_1 * poly_1 - poly_3 - poly_3
13    poly_6 = poly_2 * poly_2
14    poly_7 = poly_2 * poly_3
15    poly_8 = poly_3 * poly_1
16    poly_9 = poly_2 * poly_5
17    poly_10 = poly_2 * poly_4
18    poly_11 = poly_1 * poly_5 - poly_8
19    poly_12 = poly_2 * poly_6
20    return jnp.stack([poly_0, poly_1, poly_2, poly_3,
21                    poly_4, poly_5, poly_6, poly_7,
22                    poly_8, poly_9, poly_10, poly_11,
23                    poly_12,])

```

Listing 3. Polynomial function for A<sub>2</sub>B molecule.

```

1 from typing import Callable
2 import jax.numpy as jnp
3 from flax import linen as nn
4 from molpipx.utils import all_distances, softplus_inverse
5
6 @nn.jit
7 class PIP(nn.Module):
8     f_mono: Callable # monomials function
9     f_poly: Callable # polynomials function
10    l: float = float(1.) # morse variable
11    bias_init: Callable = nn.initializers.constant
12
13    @nn.compact
14    def __call__(self, input):
15        f_mono, f_poly = self.f_mono, self.f_poly
16        _lambda = self.param('lambda',
17                             self.bias_init(softplus_inverse(self.l)), (1,))
18        l = nn.softplus(_lambda)
19        d = all_distances(input) # distances
20        morse = jnp.exp(-l*d) # morse variables
21        return f_poly(morse) # compute PIP vector
22
23 @nn.jit
24 class PIPLayer(nn.Module):
25     f_mono: Callable
26     f_poly: Callable
27     l: float = float(jnp.exp(1))
28
29    @nn.compact
30    def __call__(self, inputs):

```

```

31 # Vectorized version of 'PIP'.
32 vmap_pipblock = nn.vmap(PIP,
33                        variable_axes={'params': None},
34                        split_rngs={'params': False},
35                        in_axes=(0,))(self.f_mono, self.f_poly, self.l)
36 return vmap_pipblock(inputs)

```

Listing 4. Flax module of the PIP layer.

One of the main motivations for using JAX as an AD back-end is the existing ML ecosystem. For the JAX back-end version,  $\Phi_{\text{PIP}}$  is defined as a Flax Module `dataclass` framework (PIPLayer), see Listing 4. Flax also facilitates the incorporation of  $\Phi_{\text{PIP}}$  into other ML libraries like GPJax for example.

To initialize the PIPLayer, it is required to provide the monomial and polynomial functions in JAX, and the value of  $\lambda$ , as shown in Listing 4. In this library, linear PIP models (Eq. 6) are defined as PIPLayer followed by a Dense layer. The extension for PIP-NN models is straightforward, we alternate an activation function with a Dense layer, as is common practice in ML libraries. For both linear PIP and PIP-NN models, the optimization of any parameter can be done with gradient-based algorithms. MOLPIPx is compatible with the Optax<sup>144</sup> and JAXopt<sup>101</sup> libraries, which contain many gradient descent algorithms commonly used for training modern ML models.

## IV. EXAMPLES

The following examples illustrate the use of all previously mentioned regression models, Section II, built-in MOLPIPx for the JAX back-end. Currently, the Rust version is limited only to linear models. However, we foresee an easy adaptation to ML libraries based on Rust-AD. A more detailed Python code of these examples can be found in <https://github.com/ChemAI-Lab/molpipx/tree/main/examples>. We use methane, A<sub>4</sub>B, molecule for all examples here. For all the results presented here, the training data was obtained from Ref.<sup>28</sup> and can be downloaded from <https://scholarblogs.emory.edu/bowman/potential-energy-surfaces/>.

### A. Linear Models Training

As mentioned in Section II B, in MOLPIPx the optimization of  $w$  (Eq. 6) currently uses `jax.numpy.linalg.lstsq`. MOLPIPx provides two additional functions, `training`, and `training_w_gradients`, the later accounts for the use of  $\nabla_x \Phi_{\text{PIP}}$ , Ref.<sup>28</sup>. The optimal weights are then copied to a Flax’s parameters Pytree structure, compatible with Flax’s Dense layer module (Listing 5).

```

1 from molpipx import PIPLayer, EnergyPIP
2 from molpipx import training
3 from molpipx import training_w_gradients, flax_params
4 # PIP models
5 pip_model = PIPLayer(f_mono, f_poly)
6 e_pip_model = EnergyPIP(f_mono, f_poly)
7 x0 = jnp.ones([1, na, 3]) # dummy geometry
8 params_pip = pip_model.init(rng, x0)
9 params_epip = e_pip_model.init(rng, x0)

```

```

10# training
11 X_tr, y_tr = load_data()
12 w_opt = training(model_pip, X_tr, y_tr) # Array
13 params_opt = flax_params(w, params) # Array to Pytree

```

Listing 5. Linear PIP models.

## B. Joint evaluation of energy and force

For scalar-valued functions, JAX enables the computation of both the function and its gradient simultaneously using the `jax.value_and_grad` function. We have adapted this tool to work with any model developed within MOLPIPx, enabling the joint computation of energy and forces. Listing 6 is a Python code snippet demonstrating the prediction of the energy and forces using the adapted `get_energy_and_forces` function.

```

1 from molpipx import get_energy_and_forces
2
3 # only energy
4 y = e_pip_model.apply(params_opt, X)
5 # energy and forces
6 y, f = get_energy_and_forces(e_pip_model.apply,
7                               X, params_opt)

```

Listing 6. Energy and force prediction.

While all models in MOLPIPx are compatible with `jax.jit` compilation to enhance performance, this optimization introduces additional computational costs. For the molecules listed in Table I, we have recorded the time required to jit the `get_energy_and_forces` function for various linear PIP models with different polynomial degrees. The subsequent prediction times post-jit are shown in Fig. 3. As we can observe, the jitting time grows with the complexity of the PIP; however, after jitting, the joint evaluation of the energy and force for  $p < 4$  is below  $10^{-3}s$ . The same trend holds using the bigger batches due to the vectorizing map function in JAX. Both jit and post-jit times for all systems were computed in a 2 x Intel(R) Xeon(R) Gold 6248R CPU 3.00GHz with 384GB memory. We do not report the jitting times for the JAX version for PIP models with  $p = 8$  as these are in the order of 10 hours when considering systems with 5 atoms. Additionally, we found the compile times for the joint computation of the energy and force using Enzyme-Rust AD in reverse mode for  $A_5$  and ABCDE, using a polynomial with degree 8, were 33.5 s and 26 minutes specifically, showcasing a promising speed up compared to the time JAX takes to jit the `value_and_grad` function.

## C. Optimization of $\lambda$ for $\Phi_{PIP}^{aniso}$

Here, we will consider the optimization of an anisotropic PIP model for an  $A_4B$  molecule, where  $\lambda = [\lambda_{AA}, \lambda_{AB}]$ , and the distance vector is

$$\mathbf{r} = [r_{A_1A_2}, r_{A_1A_3}, r_{A_1A_4}, r_{A_1B}, r_{A_2A_3}, r_{A_2A_4}, r_{A_2B}, r_{A_3A_4}, r_{A_3B}, r_{A_4B}] \quad (20)$$

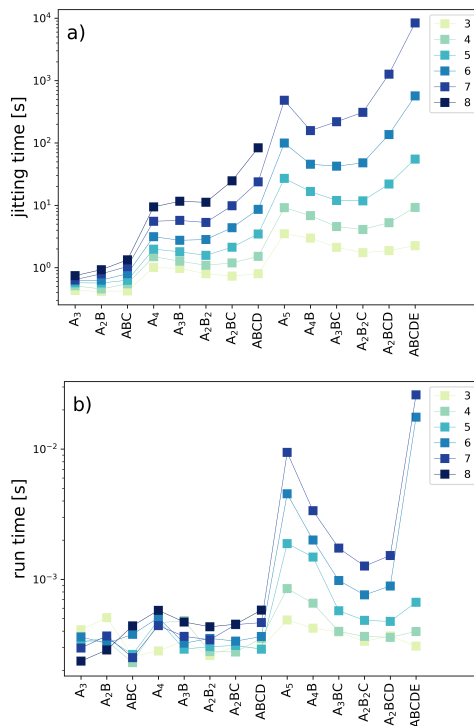


FIG. 3. Jitting times (a) and post-jitting run times (b) for the joint computation of energy and force using reverse mode differentiation. Both panels show results for polynomial degrees ranging from 3 to 8. The results for molecules with 5 atoms with  $p = 8$  are omitted, as the jitting time exceeded 5 hours. All computations were carried in a 2 x Intel(R) Xeon(R) Gold 6248R CPU 3.00GHz with 384GB memory.

For an  $A_4B$  molecule, the mask vectors ( $\omega$ ) are defined as,

$$\omega = \begin{bmatrix} \omega_{AA}^\top \\ \omega_{AB}^\top \end{bmatrix} = \begin{bmatrix} 1 & 1 & 1 & 0 & 1 & 1 & 0 & 1 & 0 & 0 \\ 0 & 0 & 0 & 1 & 0 & 0 & 1 & 0 & 1 & 1 \end{bmatrix}. \quad (21)$$

As mentioned in Section II C, the optimization of  $\lambda$  depends on the outer (validation) and inner (training) loss functions, defined as,

$$\mathcal{L}_{outer}(\lambda) = \frac{1}{N} \sum_i^N \left( \tilde{\mathbf{w}}(\lambda)^\top \Phi_{PIP}^{aniso}(\mathbf{x}_i, \lambda) - V(\mathbf{x}_i) \right)^2, \quad (22)$$

where the optimal linear parameters,  $\tilde{\mathbf{w}}(\lambda)$ , are found by solving Eq. 7, the minimizer of  $\mathcal{L}_{inner}$ . Fig. 4 illustrates the optimization trajectories of different randomly initialized  $\lambda$  for  $CH_4$  using a third-degree PIP. We considered two different scenarios, in Fig. 4 (a) the inner function only uses energy data, while in Fig. 4 (b) we used energy and forces for Eq. 7. For both simulations, the outer loss function only depends on energy data. To ensure the values of  $\lambda$  remain positive, we applied the softplus function.

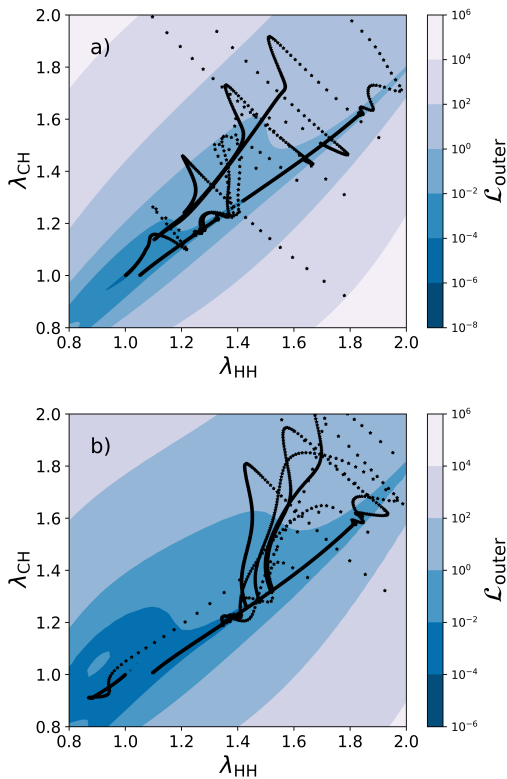


FIG. 4. Optimization trajectories of ten random initial  $\lambda$  for methane using an  $\Phi_{\text{PIP}}^{\text{aniso}}$  model with a third-degree polynomial. Both, the inner and outer loss functions used 500 data points each. (a) shows trajectories optimized with the inner loss function based solely on energy, while (b) incorporates forces. The Adam optimizer was employed with a learning rate of 0.1.

#### D. Training PIP-NN

Given the relevance of PIP-NN, we considered two examples, the tuning of the  $\lambda_0$  hyper-parameter when jointly considering forces and energies, and the number of neurons' impact on the model's accuracy.

PIP-NN has been widely employed in PESs, as discussed in Section II D. The training of PIP-NNs can include both energy and forces, as indicated in Eq. 15. Fig. 5 depicts the search for the optimal value of the  $\lambda_0$  hyper-parameter, using 1,000 training and validation data points. Our grid search protocol demonstrates that the optimal value is  $\lambda_0 = 0.1$  for a third-degree polynomial PIP-NN with two layers, each containing 128 neurons using the  $\tanh$  activation function. This value corresponds to the lowest validation error for the forces. The training was conducted using the Adam algorithm with a learning rate of  $2 \times 10^{-3}$  with a batch size of 128.

The training and validation learning curves provide insights into identifying the best-performing model. Fig. 6 (a) shows the training loss across different epochs for models with varying numbers of neurons in a three-layer architecture, based on 1,000 training energy data points for the methane molecule. Furthermore, the validation loss curve, Fig. 6 (b), helps assess

the model's generalization capability to unseen data. These results indicate that for  $\text{CH}_4$ , the best model has 128 neurons, as it smoothly converged more effectively compared to the other models.

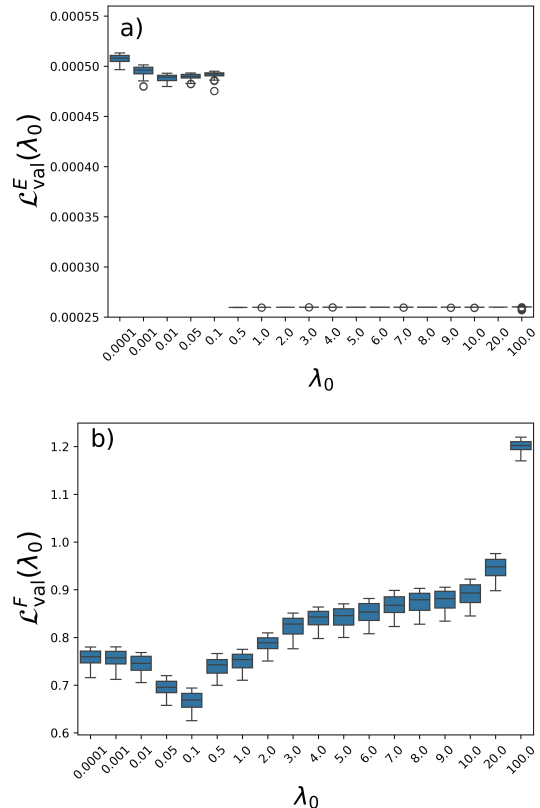


FIG. 5. (a) Bar plots of the 100 lowest validation errors for energy and (b) forces during training for methane molecule. 1,000 validation data points are considered to calculate both validation errors. For more details about the PIP-NN architecture and the training see the text.

#### E. Training PIP-GP

As previously discussed, Section II E, the kernel parameters ( $\theta$ ) in PIP-GPs are optimized by maximizing LML, Eq. 18. After determining the optimal parameters, the model can predict energy for different coordinates or geometrical configurations. Fig. 7 shows the results for  $\text{CH}_4$  using different kernel functions, with models trained on 1,000 data points and evaluated on 5,000 unseen data points. Based on our results, Fig. 7 (a), the Matern- $\frac{5}{2}$  kernel demonstrated superior performance with respect to PIP-GP with other kernels. Furthermore, Fig. 7 (b) illustrates the impact different number of training data points have on a PIP-GP with the Matern- $\frac{5}{2}$  kernel.

In GPs and PIP-GPs, the mean is tractable, therefore, we can estimate its force analytically too. Fig. 7(c) shows the  $L^2$  norm between the predicted and true forces, for 5,000 unseen data points. The compared models were trained with 1,000

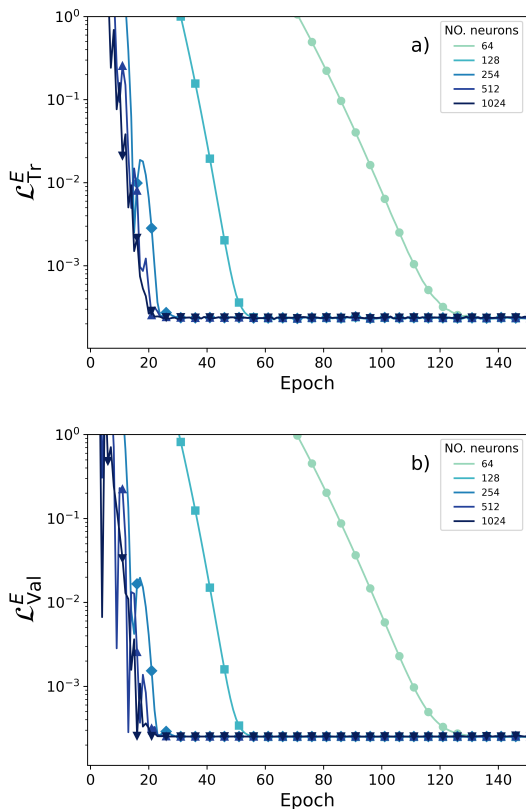


FIG. 6. (a) Training loss and (b) validation loss for energy predictions with varying numbers of neurons in a three-layer neural network for the methane molecule. The plots are based on 1,000 training and 5,000 validation data points.

data points only using energy. The energy results show that the linear PIP models with  $p = 3$  and  $p = 4$  achieve test RMSE values of 1.9 and 1.7 kcal/mol, respectively, which are more accurate than the other PIP models. A similar trend was found for predicting the forces; see Fig. 7 (c).

## V. POTENTIAL EXTENSIONS

MOLPIP $x$  is designed as a flexible library for PESs, compatible with existing machine learning frameworks such as Flax and GPJax, as well as future Rust-based libraries. Currently, MOLPIP $x$  relies on pre-existing training data and does not include built-in training or sampling protocols for each PIP-based model. However, it provides users with the flexibility to experiment with various optimization, sampling, and active learning strategies<sup>145–147</sup>. In future releases, we plan to include basic sampling and active learning algorithms to improve the overall accuracy of PES models. Additionally, we will integrate MOLPIP $x$  with existing quantum chemistry packages such as PySCF and Psi4, among others. These new features will enable users to enhance both the accuracy and utility of PES models in the study of chemical systems.

Because of the wide use of linear PIP-based models for

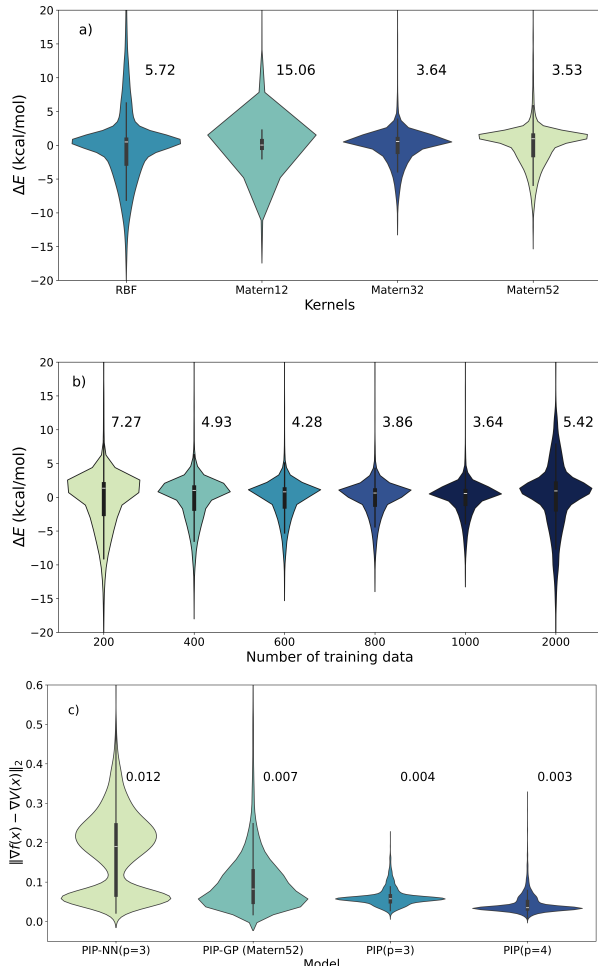


FIG. 7. (a) Comparison of different kernel functions for 1,000 training data points. (b) Performance evaluation of the PIP-GP model with the Matern- $\frac{5}{2}$  kernel using different training data points. (c) Violin plot of the  $L^2$  norm of the difference between the predicted and true forces for different models. The models were trained without force data. Experiments were carried out on the methane molecule. The numbers represent the RMSE values. All comparisons were performed using 5,000 test data points.

PESs, we aim to integrate packages like Lineax<sup>148</sup>, which offer more efficient linear solvers, and to incorporate pruning techniques, such as the L1-Lasso method, which can reduce the number of terms in the PIP vector, accelerating the computation of forces. To enhance the PIP-GP framework, we will incorporate gradients directly into the GP model, as demonstrated in previous works<sup>142,149,150</sup>. This approach will allow us to train models using both forces and energies simultaneously, leading to more accurate and robust PES fitting by fully leveraging the available data.

Looking ahead, we plan to extend the package to PyTorch<sup>151</sup>, given its status as one of the most widely used ecosystems for machine learning models. Additionally, we aim to expand the Rust-based component of the package by developing anisotropic PIPs and a simple feed forward neu-



ral networks tailored for PIP-NN. This library will also ensure compatibility with the faer-rs Rust-based linear algebra library<sup>152</sup>, thereby enhancing the versatility and adaptability of the package.

Finally, the monomial and polynomial functions listed in Table I enable the development of PESs, where PIPs are applied to each  $n$ -body term in the many-body expansion. This approach was recently employed for hydrocarbons<sup>57</sup> ( $C_{14}H_{30}$ ), where the four-body terms in the expansion were  $A_4$ ,  $A_3B$ ,  $A_2B_2$ ,  $A_2BC$ , and  $ABCD$ , as well as in the MB-pol many-body potential for water<sup>50,51</sup>. MOLPIPx could further benefit from using mask vectors, such as those utilized in the anisotropic Morse variables described in Section II C, and from the development of training schemes based on gradient-based or least-squares methods.

## VI. SUMMARY

MOLPIPx offers a comprehensive and adaptable platform that integrates PIPs with cutting-edge machine learning libraries by leveraging modern computational tools such as JAX and Enzyme-AD. Due to its end-to-end differentiable nature, MOLPIPx supports a range of regression models for PESs, from traditional linear methods to advanced models like neural networks, Gaussian Processes, and anisotropic Morse variables. Furthermore, within MOLPIPx, the computation of forces is performed automatically for any proposed PIP-based model.

We provide the monomial and polynomial functions for fifteen different molecular systems, however, MOLPIPx can be interfaced with the MSA package to translate those files into pure Python functions using JAX as the main numerical backend library. Finally, we also provide a comprehensive set of examples for each regression model to illustrate the use of MOLPIPx.

## VII. ACKNOWLEDGEMENT

The authors thank Chen Qu for fruitful discussions. MSD is thankful for the Rust Foundation’s support. This research was partly enabled by support from the Digital Research Alliance of Canada and NSERC Discovery Grant No. RGPIN-2024-06594.

## REFERENCES

- A. Brown, A. B. McCoy, B. J. Braams, Z. Jin, and J. M. Bowman, “Quantum and classical studies of vibrational motion of  $CH_5^+$  on a global potential energy surface obtained from a novel ab initio direct dynamics approach,” *The Journal of chemical physics* **121**, 4105–4116 (2004).
- G. Czako and J. M. Bowman, “Reaction dynamics of methane with F, O, Cl, and Br on ab initio potential energy surfaces,” *The Journal of Physical Chemistry A* **118**, 2839–2864 (2014).
- K. A. Peterson, S. Skokov, and J. M. Bowman, “A theoretical study of the vibrational energy spectrum of the HOCl/HClO system on an accurate ab initio potential energy surface,” *The Journal of chemical physics* **111**, 7446–7456 (1999).
- B. C. Shepler, B. J. Braams, and J. M. Bowman, “Quasiclassical trajectory calculations of acetaldehyde dissociation on a global potential energy surface indicate significant non-transition state dynamics,” *The Journal of Physical Chemistry A* **111**, 8282–8285 (2007).
- G. Czako and J. M. Bowman, “Accurate ab initio potential energy surface, thermochemistry, and dynamics of the  $Cl(^2P, ^2P_{3/2}) + CH_4 \rightarrow HCl + CH_3$  and  $H + CH_3Cl$  reactions,” *The Journal of Chemical Physics* **136** (2012).
- S. Zou and J. M. Bowman, “A new ab initio potential energy surface describing acetylene/vinylidene isomerization,” *Chemical physics letters* **368**, 421–424 (2003).
- X. Huang, S. Carter, and J. Bowman, “Ab initio potential energy surface and rovibrational energies of  $H_3O^+$  and its isotopomers,” *The Journal of chemical physics* **118**, 5431–5441 (2003).
- Z. Homayoon, R. Conte, C. Qu, and J. M. Bowman, “Full-dimensional, high-level ab initio potential energy surfaces for  $H_2(H_2O)$  and  $H_2(H_2O)$  with application to hydrogen clathrate hydrates,” *The Journal of Chemical Physics* **143**, 084302 (2015).
- X. Wang, P. L. Houston, and J. M. Bowman, “A new (multi-reference configuration interaction) potential energy surface for  $H_2CO$  and preliminary studies of roaming,” *Philosophical Transactions of the Royal Society A: Mathematical, Physical and Engineering Sciences* **375**, 20160194 (2017).
- A. R. Sharma, J. Wu, B. J. Braams, S. Carter, R. Schneider, B. Shepler, and J. M. Bowman, “Potential energy surface and MULTIMODE vibrational analysis of  $C_2H_3^+$ ,” *The Journal of chemical physics* **125**, 224306 (2006).
- X. Huang, S. Carter, and J. M. Bowman, “Ab initio potential energy surface and vibrational energies of  $H_3O^+$  and its isotopomers,” *The Journal of Physical Chemistry B* **106**, 8182–8188 (2002).
- D. Xu, H. Guo, S. Zou, and J. Bowman, “A scaled ab initio potential energy surface for acetylene and vinylidene,” *Chemical physics letters* **377**, 582–588 (2003).
- P. Pandey, C. Qu, A. Nandi, Q. Yu, P. L. Houston, R. Conte, and J. M. Bowman, “Ab initio potential energy surface for  $NaCl-H_2$  with correct long-range behavior,” *The Journal of Physical Chemistry A* **128**, 902–908 (2024).
- R. Conte, P. L. Houston, and J. M. Bowman, “Communication: A benchmark-quality, full-dimensional ab initio potential energy surface for  $Ar-HOCO$ ,” *The Journal of Chemical Physics* **140**, 151101 (2014).
- J. M. Bowman, B. J. Braams, S. Carter, C. Chen, G. Czako, B. Fu, X. Huang, E. Kamarchik, A. R. Sharma, B. C. Shepler, Y. Wang, and Z. Xie, “Ab-initio-based potential energy surfaces for complex molecules and molecular complexes,” *The Journal of Physical Chemistry Letters* **1**, 1866–1874 (2010).
- P. O. Dral, “Quantum chemistry in the age of machine learning,” *The journal of physical chemistry letters* **11**, 2336–2347 (2020).
- T. Fröhlking, M. Bernetti, N. Calonaci, and G. Bussi, “Toward empirical force fields that match experimental observables,” *The Journal of chemical physics* **152**, 230902 (2020).
- B. Jiang, J. Li, and H. Guo, “High-fidelity potential energy surfaces for gas-phase and gas-surface scattering processes from machine learning,” *The Journal of Physical Chemistry Letters* **11**, 5120–5131 (2020).
- R. Jinnouchi, K. Miwa, F. Karsai, G. Kresse, and R. Asahi, “On-the-fly active learning of interatomic potentials for large-scale atomistic simulations,” *The Journal of Physical Chemistry Letters* **11**, 6946–6955 (2020).
- D. Koner, S. M. Salehi, P. Mondal, and M. Meuwly, “Non-conventional force fields for applications in spectroscopy and chemical reaction dynamics,” *The Journal of chemical physics* **153**, 010901 (2020).
- I. Poltavsky and A. Tkatchenko, “Machine learning force fields: Recent advances and remaining challenges,” *The journal of physical chemistry letters* **12**, 6551–6564 (2021).
- Q. Tong, P. Gao, H. Liu, Y. Xie, J. Lv, Y. Wang, and J. Zhao, “Combining machine learning potential and structure prediction for accelerated materials design and discovery,” *The Journal of Physical Chemistry Letters* **11**, 8710–8720 (2020).
- J. Westermayr, M. Gastegger, K. T. Schütt, and R. J. Maurer, “Perspective on integrating machine learning into computational chemistry and materials science,” *The Journal of Chemical Physics* **154**, 230903 (2021).
- B. J. Braams and J. M. Bowman, “Permutationally invariant potential energy surfaces in high dimensionality,” *International Reviews in Physical*

- Chemistry **28**, 577–606 (2009).
- <sup>25</sup>C. Qu, Q. Yu, and J. M. Bowman, “Permutationally invariant potential energy surfaces,” *Annual review of physical chemistry* **69**, 151–175 (2018).
- <sup>26</sup>P. Pandey, M. Arandhara, P. L. Houston, C. Qu, R. Conte, J. M. Bowman, and S. G. Ramesh, “Assessing permutationally invariant polynomial and symmetric gradient domain machine learning potential energy surfaces for  $\text{H}_3\text{O}_2^+$ ,” *The Journal of Physical Chemistry A* **128**, 3212–3219 (2024).
- <sup>27</sup>T. Xie and J. M. Bowman, “On using potential, gradient, and hessian data in least squares fits of potentials: Application and tests for  $\text{H}_2\text{O}$ ,” *The Journal of chemical physics* **117**, 10487–10492 (2002).
- <sup>28</sup>A. Nandi, C. Qu, and J. M. Bowman, “Using gradients in permutationally invariant polynomial potential fitting: A demonstration for  $\text{CH}_4$  using as few as 100 configurations,” *Journal of Chemical Theory and Computation* **15**, 2826–2835 (2019).
- <sup>29</sup>R. Conte, C. Qu, P. L. Houston, and J. M. Bowman, “Efficient generation of permutationally invariant potential energy surfaces for large molecules,” *Journal of Chemical Theory and Computation* **16**, 3264–3272 (2020).
- <sup>30</sup>P. L. Houston, C. Qu, A. Nandi, R. Conte, Q. Yu, and J. M. Bowman, “Permutationally invariant polynomial regression for energies and gradients, using reverse differentiation, achieves orders of magnitude speed-up with high precision compared to other machine learning methods,” *The Journal of Chemical Physics* **156**, 044120 (2022).
- <sup>31</sup>O. T. Unke, S. Chmiela, H. E. Sauceda, M. Gastegger, I. Poltavsky, K. T. Schütt, A. Tkatchenko, and K.-R. Müller, “Machine learning force fields,” *Chemical Reviews* **121**, 10142–10186 (2021).
- <sup>32</sup>T. Murakami, S. Takahashi, Y. Kikuma, and T. Takayanagi, “Theoretical study of the thermal rate coefficients of the  $\text{H}_3^+ + \text{C}_2\text{H}_4$  reaction: Dynamics study on a full-dimensional potential energy surface,” *Molecules* **29**, 2789 (2024).
- <sup>33</sup>X. Liu, W. Wang, and J. Pérez-Ríos, “Molecular dynamics-driven global potential energy surfaces: Application to the alf dimer,” *The Journal of Chemical Physics* **159**, 144103 (2023).
- <sup>34</sup>O. T. Unke, D. Koner, S. Patra, S. Käser, and M. Meuwly, “High-dimensional potential energy surfaces for molecular simulations: from empiricism to machine learning,” *Machine Learning: Science and Technology* **1**, 013001 (2020).
- <sup>35</sup>Y. Zhang and B. Jiang, “Universal machine learning for the response of atomistic systems to external fields,” *Nature Communications* **14**, 6424 (2023).
- <sup>36</sup>J. Behler, “Neural network potential-energy surfaces in chemistry: a tool for large-scale simulations,” *Phys. Chem. Chem. Phys.* **13**, 17930–17955 (2011).
- <sup>37</sup>J. M. Bowman, C. Qu, R. Conte, A. Nandi, P. L. Houston, and Q. Yu, “ $\Delta$ -machine learned potential energy surfaces and force fields,” *Journal of Chemical Theory and Computation* **19**, 1–17 (2022).
- <sup>38</sup>A. Brown, B. J. Braams, K. Christoffel, Z. Jin, and J. M. Bowman, “Classical and quasiclassical spectral analysis of  $\text{CH}_5^+$  using an ab initio potential energy surface,” *The Journal of chemical physics* **119**, 8790–8793 (2003).
- <sup>39</sup>Z. Xie, B. J. Braams, and J. M. Bowman, “Ab initio global potential-energy surface for  $\text{H}_5^+ \rightarrow \text{H}_3^+ + \text{H}_2$ ,” *The Journal of chemical physics* **122**, 224307 (2005).
- <sup>40</sup>X. Zhang, B. J. Braams, and J. M. Bowman, “An ab initio potential surface describing abstraction and exchange for  $\text{H} + \text{CH}_4$ ,” *The Journal of chemical physics* **124**, 021104 (2006).
- <sup>41</sup>A. Nandi, C. Qu, P. L. Houston, R. Conte, and J. M. Bowman, “ $\Delta$ -machine learning for potential energy surfaces: A PIP approach to bring a DFT-based PES to CCSD(T) level of theory,” *The Journal of Chemical Physics* **154**, 051102 (2021).
- <sup>42</sup>X. Wang, S. Carter, and J. M. Bowman, “Pruning the hamiltonian matrix in MULTIMODE: Test for  $\text{C}_2\text{H}_4$  and application to  $\text{CH}_3\text{NO}_2$  using a new ab initio potential energy surface,” *The Journal of Physical Chemistry A* **119**, 11632–11640 (2015).
- <sup>43</sup>C. Qu and J. M. Bowman, “An ab initio potential energy surface for the formic acid dimer: zero-point energy, selected anharmonic fundamental energies, and ground-state tunneling splitting calculated in relaxed 1–4-mode subspaces,” *Physical Chemistry Chemical Physics* **18**, 24835–24840 (2016).
- <sup>44</sup>R. Conte, P. L. Houston, C. Qu, J. Li, and J. M. Bowman, “Full-dimensional, ab initio potential energy surface for glycine with characterization of stationary points and zero-point energy calculations by means of diffusion monte carlo and semiclassical dynamics,” *The Journal of Chemical Physics* **153**, 244301 (2020).
- <sup>45</sup>A. Nandi, C. Qu, and J. M. Bowman, “Full and fragmented permutationally invariant polynomial potential energy surfaces for trans and cis n-methyl acetamide and isomerization saddle points,” *The Journal of Chemical Physics* **151**, 084306 (2019).
- <sup>46</sup>C. Qu and J. M. Bowman, “A fragmented, permutationally invariant polynomial approach for potential energy surfaces of large molecules: Application to n-methyl acetamide,” *The Journal of Chemical Physics* **150**, 141101 (2019).
- <sup>47</sup>C. Qu, R. Conte, P. L. Houston, and J. M. Bowman, “Full-dimensional potential energy surface for acetylacetone and tunneling splittings,” *Physical Chemistry Chemical Physics* **23**, 7758–7767 (2021).
- <sup>48</sup>P. Houston, R. Conte, C. Qu, and J. M. Bowman, “Permutationally invariant polynomial potential energy surfaces for tropolone and H and D atom tunneling dynamics,” *The Journal of Chemical Physics* **153**, 024107 (2020).
- <sup>49</sup>P. L. Houston, C. Qu, Q. Yu, R. Conte, A. Nandi, J. K. Li, and J. M. Bowman, “PESPIP: Software to fit complex molecular and many-body potential energy surfaces with permutationally invariant polynomials,” *The Journal of Chemical Physics* **158**, 044109 (2023).
- <sup>50</sup>V. Babin, G. R. Medders, and F. Paesani, “Development of a “first principles” water potential with flexible monomers. II: Trimer potential energy surface, third virial coefficient, and small clusters,” *Journal of chemical theory and computation* **10**, 1599–1607 (2014).
- <sup>51</sup>S. K. Reddy, S. C. Straight, P. Bajaj, C. Huy Pham, M. Riera, D. R. Moberg, M. A. Morales, C. Knight, A. W. Götz, and F. Paesani, “On the accuracy of the MB-pol many-body potential for water: Interaction energies, vibrational frequencies, and classical thermodynamic and dynamical properties from clusters to liquid water and ice,” *The Journal of chemical physics* **145**, 194504 (2016).
- <sup>52</sup>E. Palos, S. Dasgupta, E. Lambros, and F. Paesani, “Data-driven many-body potentials from density functional theory for aqueous phase chemistry,” *Chemical Physics Reviews* **4**, 011301 (2023).
- <sup>53</sup>E. Palos, A. Caruso, and F. Paesani, “Consistent density functional theory-based description of ion hydration through density-corrected many-body representations,” *The Journal of Chemical Physics* **159**, 181101 (2023).
- <sup>54</sup>E. F. Bull-Vulpe, M. Riera, A. W. Götz, and F. Paesani, “MB-Fit: Software infrastructure for data-driven many-body potential energy functions,” *The Journal of Chemical Physics* **155**, 124801 (2021).
- <sup>55</sup>M. Riera, C. Knight, E. F. Bull-Vulpe, X. Zhu, H. Agnew, D. G. Smith, A. C. Simmonett, and F. Paesani, “MBX: A many-body energy and force calculator for data-driven many-body simulations,” *The Journal of Chemical Physics* **159**, 054802 (2023).
- <sup>56</sup>M. Riera, E. P. Yeh, and F. Paesani, “Data-driven many-body models for molecular fluids:  $\text{CO}_2/\text{H}_2\text{O}$  mixtures as a case study,” *Journal of Chemical Theory and Computation* **16**, 2246–2257 (2020).
- <sup>57</sup>J. Bowman, C. Qu, P. Houston, T. Allison, and B. Schneider, “DFT-based permutationally invariant polynomial potentials capture the twists and turns of  $\text{C}_{14}\text{H}_{30}$ ,” *Journal of Chemical Theory and Computation* **20**, 9339 (2024).
- <sup>58</sup>T. Györi and G. Czakoó, “Automating the development of high-dimensional reactive potential energy surfaces with the robosurfer program system,” *Journal of Chemical Theory and Computation* **16**, 51–66 (2019).
- <sup>59</sup>D. R. Moberg and A. W. Jasper, “Permutationally invariant polynomial expansions with unrestricted complexity,” *Journal of Chemical Theory and Computation* **17**, 5440–5455 (2021).
- <sup>60</sup>D. R. Moberg, A. W. Jasper, and M. J. Davis, “Parsimonious potential energy surface expansions using dictionary learning with multipass greedy selection,” *The Journal of Physical Chemistry Letters* **12**, 9169–9174 (2021).
- <sup>61</sup>D. Koner and M. Meuwly, “Permutationally invariant, reproducing kernel-based potential energy surfaces for polyatomic molecules: From formaldehyde to acetone,” *Journal of chemical theory and computation* **16**, 5474–5484 (2020).
- <sup>62</sup>Z. Varga and D. G. Truhlar, “Potential energy surface for high-energy  $\text{N} + \text{N}_2$  collisions,” *Physical Chemistry Chemical Physics* **23**, 26273–26284 (2021).

- <sup>63</sup>Z. Varga, Y. Liu, J. Li, Y. Paukku, H. Guo, and D. G. Truhlar, "Potential energy surfaces for high-energy N + O<sub>2</sub> collisions," *The Journal of Chemical Physics* **154**, 084304 (2021).
- <sup>64</sup>J. Li, Z. Varga, D. G. Truhlar, and H. Guo, "Many-body permutationally invariant polynomial neural network potential energy surface for N<sub>4</sub>," *Journal of Chemical Theory and Computation* **16**, 4822–4832 (2020).
- <sup>65</sup>Y. Paukku, K. R. Yang, Z. Varga, and D. G. Truhlar, "Global ab initio ground-state potential energy surface of N<sub>4</sub>," *The Journal of chemical physics* **139**, 044309 (2013).
- <sup>66</sup>R. Conte, C. Qu, and J. M. Bowman, "Permutationally invariant fitting of many-body, non-covalent interactions with application to three-body methane–water–water," *Journal of Chemical Theory and Computation* **11**, 1631–1638 (2015).
- <sup>67</sup>C. van der Oord, G. Dusson, G. Csányi, and C. Ortner, "Regularised atomic body-ordered permutation-invariant polynomials for the construction of interatomic potentials," *Machine Learning: Science and Technology* **1**, 015004 (2020).
- <sup>68</sup>A. E. Allen, G. Dusson, C. Ortner, and G. Csányi, "Atomic permutationally invariant polynomials for fitting molecular force fields," *Machine Learning: Science and Technology* **2**, 025017 (2021).
- <sup>69</sup>E. Uteva, R. S. Graham, R. D. Wilkinson, and R. J. Wheatley, "Interpolation of intermolecular potentials using gaussian processes," *The Journal of Chemical Physics* **147**, 161706 (2017).
- <sup>70</sup>R. Balan, N. Haghani, and M. Singh, "Permutation invariant representations with applications to graph deep learning," (2022), arXiv:2203.07546.
- <sup>71</sup>A. S. Abbott, J. M. Turney, B. Zhang, D. G. A. Smith, D. Altarawy, and H. F. I. Schaefer, "PES-Learn: An open-source software package for the automated generation of machine learning models of molecular potential energy surfaces," *Journal of Chemical Theory and Computation* **15**, 4386–4398 (2019).
- <sup>72</sup>J. P. Heindel, Q. Yu, J. M. Bowman, and S. S. Xantheas, "Benchmark electronic structure calculations for H<sub>3</sub>O<sup>+</sup>(H<sub>2</sub>O)<sub>n</sub>, n = 0–5, clusters and tests of an existing 1,2,3-body potential energy surface with a new 4-body correction," *Journal of Chemical Theory and Computation* **14**, 4553–4566 (2018).
- <sup>73</sup>A. Nandi, R. Conte, C. Qu, P. L. Houston, Q. Yu, and J. M. Bowman, "Quantum calculations on a new CCSD(T) machine-learned potential energy surface reveal the leaky nature of gas-phase trans and gauche ethanol conformers," *Journal of Chemical Theory and Computation* **18**, 5527–5538 (2022).
- <sup>74</sup>J. L. Bin Jiang and H. Guo, "Potential energy surfaces from high fidelity fitting of ab initio points: the permutation invariant polynomial - neural network approach," *International Reviews in Physical Chemistry* **35**, 479–506 (2016).
- <sup>75</sup>B. Jiang and H. Guo, "Permutation invariant polynomial neural network approach to fitting potential energy surfaces," *The Journal of Chemical Physics* **139**, 054112 (2013).
- <sup>76</sup>J. Li, J. Chen, D. H. Zhang, and H. Guo, "Quantum and quasi-classical dynamics of the OH + CO → H + CO<sub>2</sub> reaction on a new permutationally invariant neural network potential energy surface," *The Journal of Chemical Physics* **140**, 044327 (2014).
- <sup>77</sup>J. Li, B. Jiang, and H. Guo, "Permutation invariant polynomial neural network approach to fitting potential energy surfaces. II. four-atom systems," *The Journal of chemical physics* **139**, 204103 (2013).
- <sup>78</sup>J. Li and H. Guo, "A new ab initio based global HOOH (1<sup>3</sup>A<sup>′</sup>) potential energy surface for the O(<sup>3</sup>P) + H<sub>2</sub>O(X<sup>1</sup>A<sub>1</sub>) ⇌ OH(X<sup>2</sup>Π) + OH(X<sup>2</sup>Π) reaction," *The Journal of Chemical Physics* **138**, 074309 (2013).
- <sup>79</sup>J. Li, B. Jiang, and H. Guo, "Spin-orbit corrected full-dimensional potential energy surfaces for the two lowest-lying electronic states of FH<sub>2</sub>O and dynamics for the F + H<sub>2</sub>O → HF + OH reaction," *The Journal of Chemical Physics* **138**, 074309 (2013).
- <sup>80</sup>A. Li and H. Guo, "A nine-dimensional ab initio global potential energy surface for the H<sub>2</sub>O<sup>+</sup> + H<sub>2</sub> → H<sub>3</sub>O<sup>+</sup> + H reaction," *The Journal of Chemical Physics* **140**, 224313 (2014).
- <sup>81</sup>A. Li and H. Guo, "A full-dimensional global potential energy surface of H<sub>3</sub>O<sup>+</sup>( $\tilde{a}^3A$ ) for the OH<sup>+</sup>( $\tilde{X}^3\Sigma^-$ ) + H<sub>2</sub>( $\tilde{X}^1\Sigma_g^+$ ) → H(<sup>2</sup>S) + H<sub>2</sub>O<sup>+</sup>( $\tilde{X}^2B_1$ ) reaction," *The Journal of Physical Chemistry A* **118**, 11168–11176 (2014).
- <sup>82</sup>J. Li and H. Guo, "A nine-dimensional global potential energy surface for NH<sub>4</sub>(X<sup>2</sup>A<sub>1</sub>) and kinetics studies on the H + NH<sub>3</sub> ⇌ H<sub>2</sub> + NH<sub>2</sub> reaction," *Physical Chemistry Chemical Physics* **16**, 6753–6763 (2014).
- <sup>83</sup>J. Li and H. Guo, "Communication: An accurate full 15 dimensional permutationally invariant potential energy surface for the OH + CH<sub>4</sub> → H<sub>2</sub>O + CH<sub>3</sub> reaction," *The Journal of Chemical Physics* **143**, 221103 (2015).
- <sup>84</sup>J. Li, H. Song, and H. Guo, "Insights into the bond-selective reaction of Cl + HOD(<sub>n</sub>OH) → HCl + OD," *Physical Chemistry Chemical Physics* **17**, 4259–4267 (2015).
- <sup>85</sup>J. Li, S. Carter, J. M. Bowman, R. Dawes, D. Xie, and H. Guo, "High-level, first-principles, full-dimensional quantum calculation of the rovibrational spectrum of the simplest criegee intermediate (CH<sub>2</sub>OO)," *The Journal of Physical Chemistry Letters* **5**, 2364–2369 (2014).
- <sup>86</sup>H.-G. Yu, S. Ndengue, J. Li, R. Dawes, and H. Guo, "Vibrational energy levels of the simplest Criegee intermediate (CH<sub>2</sub>OO) from full-dimensional Lanczos, MCTDH, and MULTIMODE calculations," *The Journal of Chemical Physics* **143**, 084311 (2015).
- <sup>87</sup>J. Li and H. Guo, "Full-dimensional potential energy surface and rovibrational levels of dioxirane," *The Journal of Physical Chemistry A* **120**, 2991–2998 (2016).
- <sup>88</sup>H. Han, A. Li, and H. Guo, "Toward spectroscopically accurate global ab initio potential energy surface for the acetylene-vinylidene isomerization," *The Journal of chemical physics* **141**, 244312 (2014).
- <sup>89</sup>L. Guo, H. Han, J. Ma, and H. Guo, "Quantum dynamics of vinylidene photodetachment on an accurate global acetylene-vinylidene potential energy surface," *The Journal of Physical Chemistry A* **119**, 8488–8496 (2015).
- <sup>90</sup>B. Jiang and H. Guo, "Permutation invariant polynomial neural network approach to fitting potential energy surfaces. III. molecule-surface interactions," *The Journal of chemical physics* **141**, 034109 (2014).
- <sup>91</sup>S. Manzhos and T. J. Carrington, "Neural network potential energy surfaces for small molecules and reactions," *Chemical Reviews* **121**, 10187–10217 (2021).
- <sup>92</sup>Y. Guan, H. Guo, and D. R. Yarkony, "Neural network based quasi-diabatic hamiltonians with symmetry adaptation and a correct description of conical intersections," *The Journal of Chemical Physics* **150**, 214101 (2019).
- <sup>93</sup>C. Xie, X. Zhu, D. R. Yarkony, and H. Guo, "Permutation invariant polynomial neural network approach to fitting potential energy surfaces. IV. coupled diabatic potential energy matrices," *The Journal of chemical physics* **149**, 144107 (2018).
- <sup>94</sup>Y. Liu and J. Li, "Permutation-invariant-polynomial neural-network-based  $\Delta$ -machine learning approach: A case for the HO<sub>2</sub> self-reaction and its dynamics study," *The Journal of Physical Chemistry Letters* **13**, 4729–4738 (2022).
- <sup>95</sup>C. Qu, Q. Yu, B. L. J. Van Hoozen, J. M. Bowman, and R. A. Vargas-Hernández, "Assessing gaussian process regression and permutationally invariant polynomial approaches to represent high-dimensional potential energy surfaces," *Journal of Chemical Theory and Computation* **14**, 3381–3396 (2018).
- <sup>96</sup>W. Moses and V. Churavy, "Instead of rewriting foreign code for machine learning, automatically synthesize fast gradients," *Advances in neural information processing systems* **33**, 12472–12485 (2020).
- <sup>97</sup>W. S. Moses, V. Churavy, L. Paehler, J. Hückelheim, S. H. K. Narayanan, M. Schanen, and J. Doerfert, "Reverse-mode automatic differentiation and optimization of gpu kernels via enzyme," in *Proceedings of the international conference for high performance computing, networking, storage and analysis* (2021) pp. 1–16.
- <sup>98</sup>W. S. Moses, S. H. K. Narayanan, L. Paehler, V. Churavy, M. Schanen, J. Hückelheim, J. Doerfert, and P. Hovland, "Scalable automatic differentiation of multiple parallel paradigms through compiler augmentation," in *Proceedings of the International Conference on High Performance Computing, Networking, Storage and Analysis*, SC '22 (IEEE Press, 2022).
- <sup>99</sup>Z. Xie and J. M. Bowman, "Permutationally invariant polynomial basis for molecular energy surface fitting via monomial symmetrization," *Journal of Chemical Theory and Computation* **6**, 26–34 (2010).
- <sup>100</sup>A. G. Baydin, B. A. Pearlmutter, A. A. Radul, and J. M. Siskind, "Automatic differentiation in machine learning: a survey," *J. Mach. Learn. Res.* **18**, 5595–5637 (2017).
- <sup>101</sup>M. Blondel, Q. Berthet, M. Cuturi, R. Frostig, S. Hoyer, F. Llinares-López, F. Pedregosa, and J.-P. Vert, "Efficient and modular implicit differentia-

- tion,” *Advances in neural information processing systems* **35**, 5230–5242 (2022).
- <sup>102</sup>P. O. Dral, B. Hourahine, and S. Grimme, “Modern semiempirical electronic structure methods,” *The Journal of Chemical Physics* **160**, 040401 (2024).
- <sup>103</sup>T. Tamayo-Mendoza, C. Kreisbeck, R. Lindh, and A. Aspuru-Guzik, “Automatic differentiation in quantum chemistry with applications to fully variational Hartree–Fock,” *ACS central science* **4**, 559–566 (2018).
- <sup>104</sup>C. W. Tan, C. J. Pickard, and W. C. Witt, “Automatic differentiation for orbital-free density functional theory,” *The Journal of Chemical Physics* **158**, 124801 (2023).
- <sup>105</sup>R. A. Vargas-Hernández, K. Jorner, R. Pollice, and A. Aspuru-Guzik, “Inverse molecular design and parameter optimization with Hückel theory using automatic differentiation,” *The Journal of Chemical Physics* **158**, 104801 (2023).
- <sup>106</sup>A. de Camargo, R. T. Q. Chen, and R. A. Vargas-Hernández, “Leveraging normalizing flows for orbital-free density functional theory,” *Machine Learning: Science and Technology* **5**, 035061 (2024).
- <sup>107</sup>X. Zhang, C. Li, H.-Z. Ye, T. C. Berkelbach, and G. K. Chan, “Performant automatic differentiation of local coupled cluster theories: Response properties and ab initio molecular dynamics,” *The Journal of Chemical Physics* **161**, 014109 (2024).
- <sup>108</sup>J. M. Arrazola, S. Jahangiri, A. Delgado, J. Ceroni, J. Izaac, A. Száva, U. Azad, R. A. Lang, Z. Niu, O. Di Matteo, R. Moyard, J. Soni, M. Schuld, R. A. Vargas-Hernández, T. Tamayo-Mendoza, C. Y.-Y. Lin, A. Aspuru-Guzik, and N. Killoran, “Differentiable quantum computational chemistry with PennyLane,” arXiv:2111.09967 (2021).
- <sup>109</sup>P. A. M Casares, J. S. Baker, M. Medvidović, R. d. Reis, and J. M. Arrazola, “GradDFT: a software library for machine learning enhanced density functional theory,” *The Journal of Chemical Physics* **160**, 062501 (2024).
- <sup>110</sup>A. Dawid, J. Arnold, B. Requena, A. Gresch, M. Płodzień, K. Donatella, K. A. Nicoli, P. Stormati, R. Koch, M. Büttner, R. Okuła, G. Muñoz-Gil, R. A. Vargas-Hernández, A. Cervera-Lierta, J. Carrasquilla, V. Dunjko, M. Gabrié, P. Huembeli, E. van Nieuwenburg, F. Vicentini, L. Wang, S. J. Wetzel, G. Carleo, E. Greplová, R. Krems, F. Marquardt, M. Tomza, M. Lewenstein, and A. Dauphin, “Modern applications of machine learning in quantum sciences,” arXiv:2204.04198 (2022).
- <sup>111</sup>M. F. Kasim and S. M. Vinko, “Learning the exchange–correlation functional from nature with fully differentiable density functional theory,” *Physical Review Letters* **127**, 126403 (2021).
- <sup>112</sup>J. Schmidt, C. L. Benavides-Riveros, and M. A. Marques, “Machine learning the physical nonlocal exchange–correlation functional of density–functional theory,” *The journal of physical chemistry letters* **10**, 6425–6431 (2019).
- <sup>113</sup>R. A. Vargas-Hernández, R. T. Chen, K. A. Jung, and P. Brumer, “Fully differentiable optimization protocols for non-equilibrium steady states,” *New Journal of Physics* **23**, 123006 (2021).
- <sup>114</sup>X. Zhang and G. K. Chan, “Differentiable quantum chemistry with PySCF for molecules and materials at the mean-field level and beyond,” *The Journal of Chemical Physics* **157**, 204801 (2022).
- <sup>115</sup>C. E. Rasmussen and C. K. I. Williams, *Gaussian Processes for Machine Learning* (The MIT Press, 2005).
- <sup>116</sup>A mask vector is a binary vector used to selectively apply operations to specific elements of another vector or matrix.
- <sup>117</sup>R. Garnett, *Bayesian optimization* (Cambridge University Press, 2023).
- <sup>118</sup>R. Vargas-Hernández, Y. Guan, D. Zhang, and R. Krems, “Bayesian optimization for the inverse scattering problem in quantum reaction dynamics,” *New Journal of Physics* **21**, 022001 (2019).
- <sup>119</sup>R. A. Vargas-Hernández, “Bayesian optimization for calibrating and selecting hybrid–density functional models,” *The Journal of Physical Chemistry A* **124**, 4053–4061 (2020).
- <sup>120</sup>E. Kocer, T. W. Ko, and J. Behler, “Neural network potentials: A concise overview of methods,” *Annual review of physical chemistry* **73**, 163–186 (2022).
- <sup>121</sup>K. Shao, J. Chen, Z. Zhao, and D. H. Zhang, “Communication: Fitting potential energy surfaces with fundamental invariant neural network,” *The Journal of Chemical Physics* **145**, 071101 (2016).
- <sup>122</sup>M. van der Wilk, M. Bauer, S. John, and J. Hensman, “Learning invariances using the marginal likelihood,” in *Advances in Neural Information Processing Systems*, Vol. 31, edited by S. Bengio, H. Wallach, H. Larochelle, K. Grauman, N. Cesa-Bianchi, and R. Garnett (Curran Associates, Inc., 2018).
- <sup>123</sup>V. L. Deringer, A. P. Bartók, N. Bernstein, D. M. Wilkins, M. Ceriotti, and G. Csányi, “Gaussian process regression for materials and molecules,” *Chemical Reviews* **121**, 10073–10141 (2021).
- <sup>124</sup>J. Cui, Z. Li, and R. V. Krems, “Gaussian process model for extrapolation of scattering observables for complex molecules: From benzene to benzonitrile,” *The Journal of chemical physics* **143**, 154101 (2015).
- <sup>125</sup>R. A. Vargas-Hernández and R. V. Krems, “Physical extrapolation of quantum observables by generalization with gaussian processes,” *Machine Learning Meets Quantum Physics*, 171–194 (2020).
- <sup>126</sup>H. Sugisawa, T. Ida, and R. V. Krems, “Gaussian process model of 51-dimensional potential energy surface for protonated imidazole dimer,” *The Journal of Chemical Physics* **153**, 114101 (2020).
- <sup>127</sup>B. Kolb, P. Marshall, B. Zhao, B. Jiang, and H. Guo, “Representing global reactive potential energy surfaces using gaussian processes,” *The Journal of Physical Chemistry A* **121**, 2552–2557 (2017).
- <sup>128</sup>A. Denzel and J. Kästner, “Gaussian process regression for geometry optimization,” *The Journal of Chemical Physics* **148**, 094114 (2018).
- <sup>129</sup>J. Cui and R. V. Krems, “Efficient non-parametric fitting of potential energy surfaces for polyatomic molecules with gaussian processes,” *Journal of Physics B: Atomic, Molecular and Optical Physics* **49**, 224001 (2016).
- <sup>130</sup>A. Christianen, T. Karman, R. A. Vargas-Hernández, G. C. Groenenboom, and R. V. Krems, “Six-dimensional potential energy surface for NaK–NaK collisions: Gaussian process representation with correct asymptotic form,” *The Journal of chemical physics* **150**, 064106 (2019).
- <sup>131</sup>J. Dai and R. V. Krems, “Interpolation and extrapolation of global potential energy surfaces for polyatomic systems by gaussian processes with composite kernels,” *Journal of Chemical Theory and Computation* **16**, 1386–1395 (2020).
- <sup>132</sup>J. Dai and R. V. Krems, “Quantum gaussian process model of potential energy surface for a polyatomic molecule,” *The Journal of Chemical Physics* **156**, 184802 (2022).
- <sup>133</sup>J. Dai and R. V. Krems, “Neural network gaussian processes as efficient models of potential energy surfaces for polyatomic molecules,” *Machine Learning: Science and Technology* **4**, 045027 (2023).
- <sup>134</sup>G. Laude, D. Calderini, D. P. Tew, and J. O. Richardson, “Ab initio instanton rate theory made efficient using gaussian process regression,” *Faraday Discuss.* **212**, 237–258 (2018).
- <sup>135</sup>A. Kamath, R. A. Vargas-Hernández, R. V. Krems, T. Carrington, and S. Manzhos, “Neural networks vs gaussian process regression for representing potential energy surfaces: A comparative study of fit quality and vibrational spectrum accuracy,” *The Journal of chemical physics* **148**, 241702 (2018).
- <sup>136</sup>R. A. Vargas-Hernández and J. R. Gardner, “Gaussian processes with spectral delta kernel for higher accurate potential energy surfaces for large molecules,” arXiv:2109.14074 (2021).
- <sup>137</sup>S. Y. Yafu Guan and D. H. Zhang, “Construction of reactive potential energy surfaces with gaussian process regression: active data selection,” *Molecular Physics* **116**, 823–834 (2018).
- <sup>138</sup>A. G. Wilson, Z. Hu, R. Salakhutdinov, and E. P. Xing, “Deep kernel learning,” in *Proceedings of the 19th International Conference on Artificial Intelligence and Statistics*, Proceedings of Machine Learning Research, Vol. 51, edited by A. Gretton and C. C. Robert (PMLR, Cadiz, Spain, 2016) pp. 370–378.
- <sup>139</sup>J. Gardner, G. Pleiss, K. Q. Weinberger, D. Bindel, and A. G. Wilson, “Gpytorch: Blackbox matrix–matrix gaussian process inference with gpu acceleration,” *Advances in neural information processing systems* **31**, 7587–7597 (2018).
- <sup>140</sup>T. Pinder and D. Dodd, “GPJax: A gaussian process framework in jax,” *Journal of Open Source Software* **7**, 4455 (2022).
- <sup>141</sup>R.-R. Griffiths, L. Klärner, H. Moss, A. Ravuri, S. Truong, Y. Du, S. Stanton, G. Tom, B. Rankovic, A. Jamasb, et al., “GAUCHE: A library for Gaussian processes in chemistry,” *Advances in Neural Information Processing Systems* **36**, 76923–76946 (2023).
- <sup>142</sup>S. Chmiela, A. Tkatchenko, H. E. Sauceda, I. Poltavsky, K. T. Schütt, and K.-R. Müller, “Machine learning of accurate energy-conserving molecular force fields,” *Science advances* **3**, e1603015 (2017).
- <sup>143</sup>K. Asnaashari and R. V. Krems, “Gradient domain machine learning with composite kernels: improving the accuracy of pes and force fields for

- large molecules,” *Machine Learning: Science and Technology* **3**, 015005 (2021).
- <sup>144</sup>DeepMind, I. Babuschkin, K. Baumli, A. Bell, S. Bhupatiraju, J. Bruce, P. Buchlovsky, D. Budden, T. Cai, A. Clark, I. Danihelka, A. Dedieu, C. Fantacci, J. Godwin, C. Jones, R. Hemsley, T. Hennigan, M. Hessel, S. Hou, S. Kapturowski, T. Keck, I. Kemaev, M. King, M. Kunesch, L. Martens, H. Merzic, V. Mikulik, T. Norman, G. Papamakarios, J. Quan, R. Ring, F. Ruiz, A. Sanchez, L. Sartran, R. Schneider, E. Sezener, S. Spencer, S. Srinivasan, M. Stanojević, W. Stokowiec, L. Wang, G. Zhou, and F. Viola, “The DeepMind JAX Ecosystem,” (2020).
- <sup>145</sup>G. S. Jung, J. Y. Choi, and S. M. Lee, “Active learning of neural network potentials for rare events,” *Digital Discovery* **3**, 514–527 (2024).
- <sup>146</sup>T. D. Loeffler, T. K. Patra, H. Chan, M. Cherukara, and S. K. Sankaranarayanan, “Active learning the potential energy landscape for water clusters from sparse training data,” *The Journal of Physical Chemistry C* **124**, 4907–4916 (2020).
- <sup>147</sup>J. Qi, T. W. Ko, B. C. Wood, T. A. Pham, and S. P. Ong, “Robust training of machine learning interatomic potentials with dimensionality reduction and stratified sampling,” *npj Computational Materials* **10**, 43 (2024).
- <sup>148</sup>J. Rader, T. Lyons, and P. Kidger, “Lineax: unified linear solves and linear least-squares in JAX and Equinox,” *AI for science workshop at Neural Information Processing Systems 2023*, arXiv:2311.17283 (2023).
- <sup>149</sup>S. Chmiela, H. E. Sauceda, K.-R. Müller, and A. Tkatchenko, “Towards exact molecular dynamics simulations with machine-learned force fields,” *Nature Communications* **9**, 3887 (2018).
- <sup>150</sup>S. Chmiela, H. E. Sauceda, I. Poltavsky, K.-R. Müller, and A. Tkatchenko, “sgdml: Constructing accurate and data efficient molecular force fields using machine learning,” *Computer Physics Communications* **240**, 38–45 (2019).
- <sup>151</sup>A. Paszke, S. Gross, F. Massa, A. Lerer, J. Bradbury, G. Chanan, T. Killeen, Z. Lin, N. Gimelshein, L. Antiga, A. Desmaison, A. Köpf, E. Yang, Z. DeVito, M. Raison, A. Tejani, S. Chilamkurthy, B. Steiner, L. Fang, J. Bai, and S. Chintala, “Pytorch: An imperative style, high-performance deep learning library,” *Advances in neural information processing systems* **32** (2019).
- <sup>152</sup>S. El Kazdadi, “faer-rs,” <https://github.com/sarah-ek/faer-rs>.